ELSEVIER

Contents lists available at ScienceDirect

Earth and Planetary Science Letters

journal homepage: www.elsevier.com/locate/epsl



A 20-million-year reconstruction to decipher the enigmatic Cambrian extinction – Ordovician biodiversification transition



Leibo Bian a,b , Anthony Chappaz c , Niels H. Schovsbo d , Xiaomei Wang a , Wenzhi Zhao a,* , Hamed Sanei b,*

- a Research Institute of Petroleum Exploration and Development, PetroChina, Beijing 100083, China
- ^b Lithospheric Organic Carbon (LOC) Group, Department of Geoscience, Aarhus University, Aarhus 8000C, Denmark
- ^c STARLAB, Department of Earth and Atmospheric Sciences, Central Michigan University, Mount Pleasant, MI 48859, USA
- d Department of Reservoir Geology, Geological Survey of Denmark and Greenland, Copenhagen 1316, Denmark

ARTICLE INFO

Article history: Received 30 December 2022 Received in revised form 1 April 2023 Accepted 12 April 2023 Available online 25 April 2023 Editor: B. Wing

Keywords: redox condition dynamics water circulation paleo environmental reconstruction Baltoscandian Basin Cambro-Ordovician

ABSTRACT

The late Cambrian extinction – Early Ordovician biodiversification represents one of the crucial lower Paleozoic biological changes. However, the mechanisms responsible for this transition remain poorly understood. Here, we reconstructed the paleoenvironmental changes based on a model that integrated the atmospheric-oceanic-biological inputs and provided the first detailed assessment of the Cambro-Ordovician biological turnover. The results show depositional environments evolved into extremely sulfidic conditions with lower nutrient inputs and more restricted water circulation from the Miaolingian to early Furongian, leading to the Steptoean Positive Carbon Isotope Excursion event. The intense volcanic activity in the early Jiangshanian appears to be responsible for the recurrent bio-calamity. Later in the mid-late Furongian (mid-Jiangshanian to Stage 10), enhanced terrestrial weathering contributed to the Earth's cooling and higher inputs of terrestrial nutrients, beneficial to the subsequent biological recovery. In the Early Ordovician and despite reduced terrestrial nutrient input, massive oceanic water upwelling alleviated sulfidic conditions and brought nutrients, laying the foundation for the Great Ordovician Biodiversification Event.

© 2023 The Author(s). Published by Elsevier B.V. This is an open access article under the CC BY license (http://creativecommons.org/licenses/by/4.0/).

1. Introduction

The late Cambrian-Early Ordovician interval (500 - 480 Ma) is a significant period in Earth's history connecting the late Cambrian extinction and the onset of the Ordovician biodiversification (Fan et al., 2020). During the late Cambrian, major environmental changes occurred, such as atmospheric oxygenation, global oceanic anoxia, volcanic activity, and polar wander events (Gill et al., 2011; Saltzman et al., 2011, 2015; Jiao et al., 2018; Krause et al., 2018; Bian et al., 2022a). These environmental changes were concomitant with important biological alterations. A major extinction of approximately half of global species took place during the late Cambrian (Fan et al., 2020). In addition, the global marine metazoan generic diversity shows a decline in the Paibian and an increase during the mid-late Jiangshanian (Rasmussen et al., 2019; Zhao et al., 2022). The following Ordovician biodiversification event is one of the greatest radiations of life in Earth's history and exhibits approxi-

mately a threefold growth in species diversity (Harper and Servais, 2018; Fan et al., 2020). Previous studies suggested that the onset of the Great Ordovician Biodiversification Event (GOBE) clearly started as early as during Early Ordovician (if not Furongian) time (Harper et al., 2020). Several causes to explain this life explosion were proposed such as ocean cooling (Trotter et al., 2008), intensified water circulation (Kröger, 2018), and increased plankton production (Trubovitz and Stigall, 2016). However, the environmental conditions that encompassed the transition from the late Cambrian extinction to the Early Ordovician biodiversification remain largely unknown

Biological proliferation and extinction events were controlled by complex processes such as variations in nutrient supply and oxygen content (Lyons et al., 2021; Chen et al., 2022; Evans et al., 2022). Within modern oceans, major inputs of nutrients increase biological productivity resulting in higher oxygen demand (Reinhard et al., 2016; Breitburg et al., 2018; Schobben et al., 2020). Oxygen-depleted conditions (hypoxia, anoxia and euxinia) in the water column are the consequence of this well-known phenomenon (Lu et al., 2016; Oschlies et al., 2018). Global warming can accelerate oceanic anoxia through reducing oxygen solubility

^{*} Corresponding authors.

E-mail addresses: zwz@petrochina.com.cn (W. Zhao), sanei@geo.au.dk (H. Sanei).

(Zhang et al., 2018; Slater et al., 2019). Changes in water circulation patterns (open vs. restricted basins) also contribute to anoxia by diminishing exchange rate of oxygenated water (Meyer and Kump, 2008; Nishioka et al., 2020; Pohl et al., 2021). Investigating the controls on the development of anoxia, nutrient availability, water circulation, and surface temperature, is necessary if we hope to have a full grasp of the processes that led to the shift between biological extinction and recovery (Laakso and Schrag, 2014; Reinhard et al., 2017).

The Baltoscandian Basin has been widely examined because it is a representative site for studying the late Cambrian atmospheric, oceanic, and biological turnover due to the well-known paleooceanography and consistent water connection with the Iapetus Ocean (Fig. 1; Sturesson et al., 2005; Gill et al., 2011, 2021; Nielsen and Schovsbo, 2015; LeRoy and Gill, 2019; Bian et al., 2022a; Zhao et al., 2022). To reconstruct paleoenvironmental changes that affected the Baltoscandian Basin, various geochemical proxies were measured on two thermally immature-low mature Alum Shale cores (Supplementary Information). Our objectives were to (1) to characterize the late Cambrian - Early Ordovician environmental changes in the Baltoscandian Basin over a 20-million-year period, and (2) to connect our new findings with the environmentalbiological coevolution occurred globally. By comparing the carbon and sulfur isotopic signatures previously reported for many locations with our new dataset, we propose a new model that brings together synchronous atmospheric-tectonic-oceanic changes and their influence on biological turnover.

2. Geological background

The Alum Shale Formation was deposited in the western margin of the Baltoscandian Basin (Fig. 1; Nielsen and Schovsbo, 2015). The depositional area of this shale covers \sim 100, 000 km² and is widely distributed across northern Europe including Denmark, Estonia, Norway, Poland, Russia, and Sweden (Fig. 1; Bian et al., 2021). The depositional period took place from the Miaolingian (Drumian) to Early Ordovician (Tremadocian). The lithology in the Alum Shale Formation is relatively homogeneous organicrich shale. The content of carbonate concretion in this formation is low in outboard areas (Nielsen and Schovsbo, 2015). The sedimentation rate was extremely low (mm scale per ka), and the depositional condition was starved (Supplementary Information and Fig. S1; Gill et al., 2021; Zhao et al., 2022). The maximum thickness of the Alum Shale is 180 m observed in the Terne-1 well (GPS coordinates: 56.344167N; 11.505556E) of Denmark and decreases towards the northwestern part of Scandinavia (Schovsbo et al., 2014). The Alum Shale has high organic matter contents with a maximum value of 28 wt% and displays extremely high concentrations of redox-sensitive metals such as Mo, U, and V (Sanei et al., 2014; Bian et al., 2021). The onset of the Alum Shale deposition was related to the formation of a submarine sill that restricted the bottom water circulation (Nielsen and Schovsbo, 2015). However, the late Cambrian - Early Ordovician water circulation between the Baltoscandian Basin and the Iapetus Ocean was persistent (Sturesson et al., 2005; Gill et al., 2021).

3. Materials and methods

3.1. Materials

Two cores were studied: the Ottenby-2 core (GPS coordinates: 56.14741N, 16.244316E) in South Öland, southeastern Sweden, and the DBH 15/73 core (GPS coordinates: 58.241896N, 13.46498E) in Mount Billingen Västergötland, central Sweden (Fig. 1B). A detailed description of Ottenby-2 core can be found in Bian et al. (2021). Within this core, phosphorus (P) and pyrite sulfur isotopes are

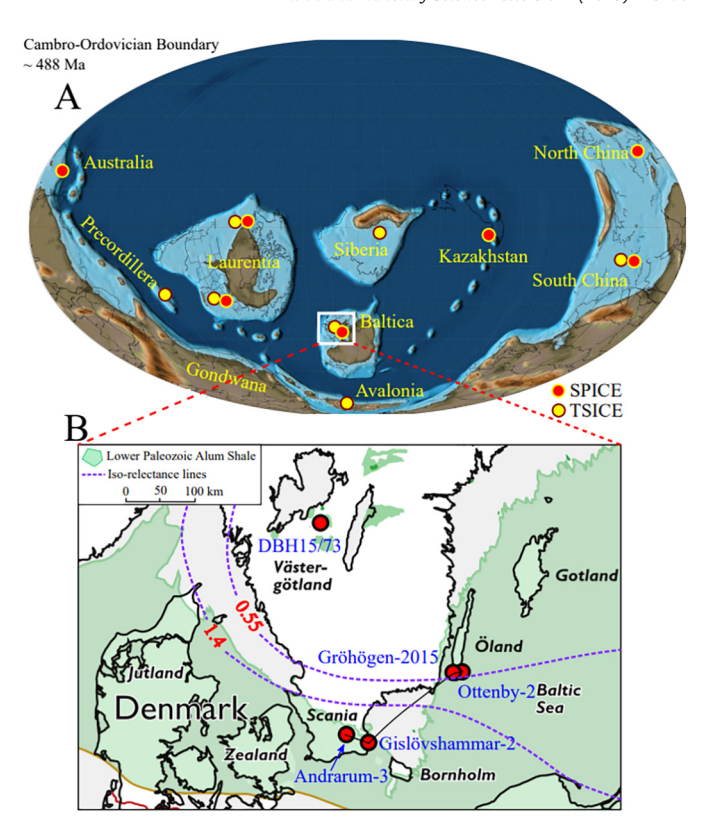


Fig. 1. A: Paleogeographic reconstruction of the Cambro-Ordovician Earth (Scotese, 2014). Red dots show the locations of reported sulfur isotope excursions during the Furongian Steptoean Positive Carbon Isotope Excursion (SPICE) event (Saltzman et al., 2000; Gill et al., 2011; LeRoy and Gill, 2019; Wotte and Strauss, 2015; Zhang et al., 2022) and yellow dots show the locations of reported sulfur isotope excursions during the Early Ordovician Top Skullrockian Isotopic Carbon Excursion (TSICE) event (Thompson and Kah, 2012; Pokrovsky et al., 2018; Edwards, 2019; Edwards et al., 2019; Todd et al., 2019; Chen et al., 2020). *B*: Locations of the Alum Shale cores as well as the iso-reflectance lines of vitrinite-like particles showing the thermal maturity of the Alum Shale Formation (Schovsbo et al., 2014; Zhao et al., 2022). The studied Ottenby-2 and DBH15/73 cores are shown.

newly provided. The other bulk dataset was compiled from Bian et al. (2021, 2022a, and 2022b). The DBH 15/73 core was never investigated until this study (Fig. 2). During the Drumian (mid Miaolingian), the lithology of DBH 15/73 core shows dark greyish shale within the *Paradoxides Paradoxissimus* Superzone and then changes to limestone in the *Goniagnostus nathorsti* Zone. After that, the lithology remains as black shale within the *Paradoxides forchhammeri* Superzone of Guzhangian (late Miaolingian). Within the Paibian-Jiangshanian Stage (early-mid Furongian), the lithology is mostly composed of the Kakeled Limestone and the stratigraphy is highly condensed. In the Stage 10 (late Furongian), it consists of black shale intercalated by carbonate concretions (Fig. 2; Supplementary text). A further description of these two cores and all relevant data is available in the Supplementary Information (Supplementary Note 1 and Tables).

3.2. Methods

A total of 197 samples were pulverized to fine-grain size using a corundum mortar at the Department of Geoscience, Aarhus University (AU), and were subsequently homogenized and separated into different aliquots for the following experiments.

3.2.1. Total organic carbon

Approximately 50-mg aliquots were used to determine total organic carbon (TOC) content through the Hawk Pyrolysis (Wildcat Technologies) at AU. Each sample was heated at an isothermal tem-

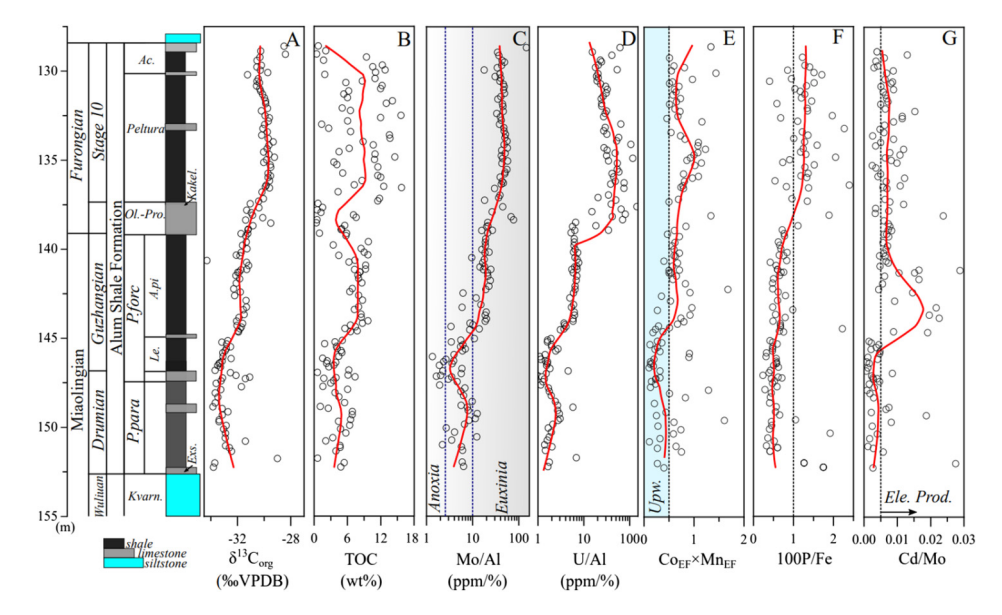


Fig. 2. Profiles showing trilobite/graptolite biozones, organic carbon isotope ($\delta^{13}C_{org}$), total organic carbon (TOC), Mo/Al, U/Al, Co_{EF}×Mn_{EF}, 100P/Fe, and Cd/Mo in the DBH 15/73 core. Within the biozones: *P.para*.: *Paradoxides paradoxissimus*; *P.forc*.: *Paradoxides forchammeri*; *Le*.: *Lejopyge laevigata*; *A.pi*.: *Agnostus pisiformis*; *Ol.- Pro*.: *Olenus-Protopeltura*; and *Ac*.: *Acerocarina*. Within the lithostratigraphy: *Kvarn*.: *Kvarntorp Member* (*sandstone*), *Kakel*.: *Kakeled Limestone Bed*, and *Exs.*: *Exsulans Limestone Bed*. In Panel E: Upw.: Upwelling. In Panel G, Ele. Prod.: Elevated productivity. In Panels A to F: the red curves are calculated using a Lowess smoothing (α = 0.15) by the PAST software package.

perature of 300 °C for 3 min to generate free hydrocarbon (S_1) and then was progressively increased to 650 °C at a rate of 25 °C/s to generate potential hydrocarbon (S_2). After that, the heating system started from an isothermal temperature of 300 °C for 1 min, followed by a gradual increase to 850 °C at a rate of 25 °C/s and held for 5 min. This process can generate oxygen-organic carbon (S_3) and residual carbon (S_4). The sum of generated S_1 , S_2 , S_3 , and S_4 is the final TOC content (Lafargue et al., 1998). The analytical uncertainties were controlled by references (the WT2 of the Wildcat Technologies, USA, and IFP 160 000 of the Vinci Technologies, France) and replicates (data precision is better than 5%).

3.2.2. Elemental analysis

Elements were measured through the Inductively Coupled Plasmas Mass Spectrometry (ICP-MS) at the ACME Lab, Vancouver. About 150-mg aliquots were digested into a multi-acid solution (hydrofluoric acid, hydrochloric acid, perchloric acid, and nitric acid). After that, the solutions were dried, and the residues were used for elemental measurement. Analytical uncertainties were controlled by reference materials (OREAS 45-E, BCR-2, and BHVO-2), replicates (\pm 7%), and blanks. The enrichment factor of each element was calibrated by the Post Archean Australia Shale composition through the equation: $X_{EF} = [(X/AI)_{sample}/(X/AI)_{PAAS}]$ (Taylor and McLennan, 1985; Babos et al., 2019).

3.2.3. Organic carbon isotopes

Organic carbon isotopes were analyzed by the isotope mass spectrometer (FermoFinnigan MAT 263 Plus) at the Department of Geoscience, Northwest University. Around 1-g aliquots were acidified with 6N HCl for 24 h. After that, the solutions were buffered to a neutral PH, filtered, and dried at 75 °C. The final residues were weighed into tin capsules that were combusted at 950 °C in a heating system to generate carbon dioxides for organic carbon isotope measurements. Analytical uncertainties were controlled by standard references (GBW 04407 and 04495) and replicates (\pm 0.3%). The final organic carbon isotope is denoted as ($\delta^{13} C_{\rm org}$) in per mil, and final values are relative to the Vienna Pee Dee Belemnite (V-PDB) reference.

3.2.4. Pyrite sulfur isotopes

Approximately 150-mg samples mixed with ethanol (10 mL) were placed in a reaction vessel, and then around 50 mL of 1M CrCl₂ solution, followed by 20 mL 6M HCl, was added through a rubber septum under the nitrogen stream. This mixed solution was then heated at 200 °C for 2 h. The H₂S generated was subsequently trapped by the AgNO₃ solution and converted into Ag₂S for sulfur isotope analyses. The sulfur isotopes were measured by an Elemental Analyzer coupled to an Isotope Ratio Mass Spectrometer (EA-IRMS) at the Institute of Geochemistry, Chinese Academy of Science. The final value is relative to the standard Vienna-Canyon Diablo Troilite (V-CDT), expressed as delta notation (δ^{34} S_{py}) in per mil. Data precision and accuracy were checked by international standard samples (IAEA S1, S2, and S3), replicates (\pm 0.5‰), and blanks.

4. Results

4.1. Chemo-stratigraphy of DBH 15/73 core

Organic carbon isotopes ($\delta^{13}C_{org}$) decrease from -32% to -33% within the Drumian *Paradoxides paradoxissimus* Superzone (Fig. 2A). Within the Guzhangian, the $\delta^{13}C_{org}$ increases to -32% within the *Lejopyge laevigate* Zone and then stays stable at around -32% within the *Agnostus pisiformis* Zone. After that, the $\delta^{13}C_{org}$ gradually increases to -30% within the Paibian-Jiangshanian Stage, and exhibits a continuous rise to around -29% in the early part of *Peltura* biozone, followed by a decrease in the *Acerocarina* Zone of Stage 10.

During the Drumian, TOC contents mainly vary between 4 and 5 wt% (Fig. 2B). After that, TOC contents remain around 4 wt% in the early Guzhangian, followed by a continuous increase to 8 wt%, and then stay stable. In the early-mid Furongian, the TOC contents show a decrease and mainly vary below 6 wt%. During the Stage 10, the TOC contents remain relatively stable at around 9 wt%, mainly varying between 5 and 12 wt% within the *Peltura* Superzone. This is followed by a rapid decrease from 12 wt% to around 1 wt% within the *Acerocarina* Zone.

The Mo/Al ratio increases from \sim 4 to \sim 10 ppm/% and then decreases to around 2 ppm/% within the Drumian (Fig. 2C). Af-

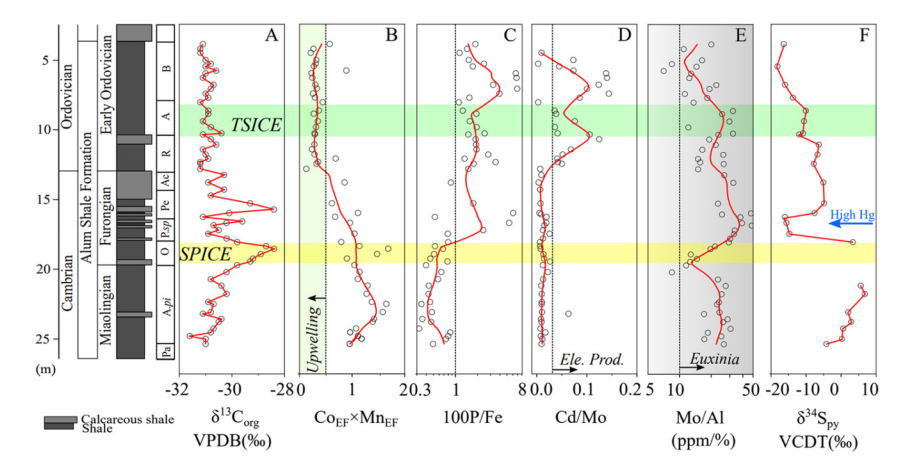


Fig. 3. Profile showing trilobite/graptolite biozones, $\delta^{13}C_{org}$, $C_{oEF} \times Mn_{EF}$, 100P/Fe, Cd/Mo, Mo/Al, pyrite sulfur isotope ($\delta^{34}S_{py}$) in the Ottenby-2 core. The $\delta^{13}C_{org}$ and Cd/Mo are compiled from Bian et al. (2022b) and the trilobite/graptolite biozones are from Bian et al. (2021). Within the biozones: Pa: *Paradoxides*; A. pi: *Agnostus pisiformis*; O: *Olenus*; Psp: *Parabolina spinulosa*; Pe: *Peltura*; Ac: *Acerocare*; R: *Rhabdinopora*; A: *Adelograptus tenellus*; and B: *Brygraptus/Kiaerograptus*. In Panel D, Ele. Prod.: Elevated productivity. The TSICE is the abbreviation of 'Top Skullrockian Isotope Carbon Excursion' and SPICE means 'Steptoean Positive Carbon Isotope Excursion'. In Panels B to E: the red smooth curves are calculated using a Lowess smoothing ($\alpha = 0.15$) by the PAST software package.

ter that, the ratio shows a continuous increase from \sim 2 to \sim 10 ppm/% and then remains above 10 ppm/% within the Guzhangian Stage. During the Furongian, the Mo/Al ratio increases from \sim 20 to \sim 30 ppm/% during the early-mid Furongian and then remains above 30 ppm/% during the late Furongian. The U/Al ratio displays an increase from \sim 1.5 to \sim 2.5 ppm/%, followed by a decrease back to \sim 1.5 ppm/% (Fig. 2D). Within the Guzhangian, U exhibits a gradual increase to \sim 6 ppm/% and then stays at this level. After that, U/Al increases to \sim 50 ppm/%, followed by a consistent decrease to \sim 10 ppm/% at the end of Furongian.

The products of Coef and Mnef (Coef and Mnef) are investigated for water circulation (Sweere et al., 2016). This proxy was developed using modern organic-rich sediments from various environments and has the potentials to characterize paleo depositional conditions (e.g., Algeo and Li, 2020; Bennett and Canfield, 2020). The $Co_{EF} \times Mn_{EF}$ values are below 0.5 during the Drumian and early Guzhangian, and then remain between 0.5 and 2 from the late Miaolingian to Furongian (Fig. 2E). The phosphorus/iron (P/Fe) ratios are used to examine biological P availability (Planavsky et al., 2010). The 100P/Fe ratios remain \sim 0.5 during the Miaolingian and then increase to above 1 during the Furongian (Fig. 2F). The cadmium/Mo (Cd/Mo) ratio was used to examine the productivity and preservation of organic matter (Sweere et al., 2016). The Cd/Mo ratios are below ~ 0.005 in the Drumian and early Guzhangian (Leiopyge laevigate Zone). After that, the Cd/Mo ratios increase to \sim 0.02, followed by a decrease to above \sim 0.005 during the late Guzhangian. The Cd/Mo ratios stay \sim 0.007 during the Furongian (Fig. 2G).

4.2. Chemo-stratigraphy of Ottenby-2 core

The $Co_{EF} \times Mn_{EF}$ values increase to $\sim\!2$ and then decrease gradually to 0.5 during the Furongian (Fig. 3). During the Early Ordovician, the $Co_{EF} \times Mn_{EF}$ values remain under $\sim\!0.5$. The P/Fe ratios are below $\sim\!1$ from the Guzhangian to Paibian, whereas they quickly increase to above $\sim\!1$ from the Jiangshanian (mid Furongian) to Tremadocian (Early Ordovician). The Cd/Mo ratios remain constant ($\sim\!0.01$) during the Miaolingian and Furongian and increase to above $\sim\!0.3$ during the Tremadocian. The Mo/Al ratios remain between 20 and 30 ppm/% during the late Miaolingian. Within the early Furongian, the Mo/Al ratios increase from 10 to $\sim\!40$ ppm/%. After that, the Mo/Al ratios decrease progressively from $\sim\!40$ to $\sim\!10$ ppm/%.

Pyrite sulfur isotopes ($\delta^{34}S_{py}$) demonstrate an upward increase ranging from approximately -5% to +5% in the Miaolingian and

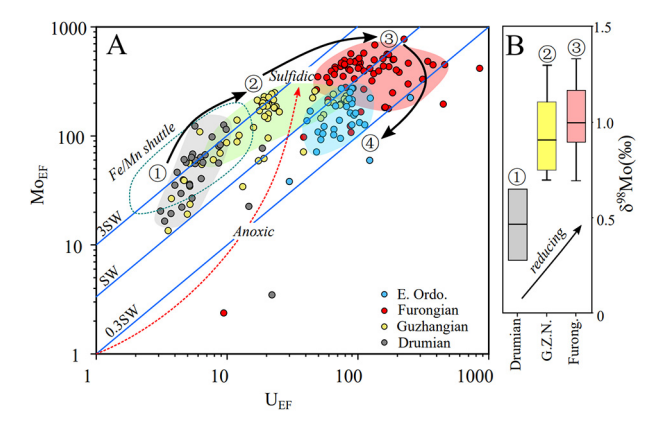


Fig. 4. A: Molybdenum (enrichment factor) versus Uranium (enrichment factor) for the Miaolingian – Early Ordovician transition in the Baltoscandian Basin (modified from Algeo and Tribovillard, 2009). ①: Drumian; ② Guzhangian; ③ Furongian; and ④ Early Ordovician (Tremadocian). The blue lines show Mo/U molar ratios equal to the seawater value (SW) and to fractions thereof (0.3SW and 3SW; Tribovillard et al., 2012). The dark green dash line shows the area for Mo accumulation triggered by the Fe/Mn shuttle. E. Ord.: Early Ordovician. Taken together this data displays the redox conditions changed drastically from the Miaolingian (Drumian) to Early Ordovician (Tremadocian). B: Molybdenum isotopes (δ^{98} Mo) measured samples from the Alum Shale supporting the evidence that the intensity of the reducing conditions increased from the Drumian to Furongian (modified from Gill et al., 2021). G.Z.N.: Guzhangian, and Furong:: Furongian.

then quickly decrease in the aftermath of the *Olenus* Superzone. The $\delta^{34} S_{py}$ values remain \sim -17‰ within the *Parabolina spinulosa* Superzone, followed by an immediate rise toward \sim -5‰. In the Early Ordovician, the $\delta^{34} S_{py}$ values remain relatively stable (\sim -6‰), and is followed by a negative \sim 5‰ excursion in the boundary of *Rhabdinopora* and *Adelograptus tenellus* graptolite zones. After that, it decreases gradually towards \sim -18‰ at \sim 5 m (Fig. 3).

5. Discussion

5.1. Baltoscandian environmental reconstruction

5.1.1. Redox conditions

Plotting U versus Mo enrichment factors is widely used to investigate the depositional redox conditions and identify the occurrence of the Fe-Mn shuttle (Algeo and Tribovillard, 2006; Rico et al., 2019). Our results show that redox conditions during the Drumian oscillated between anoxic and sulfidic conditions (Figs. 2C and 4A) and that the Fe/Mn shuttle mechanism promoted Mo ac-

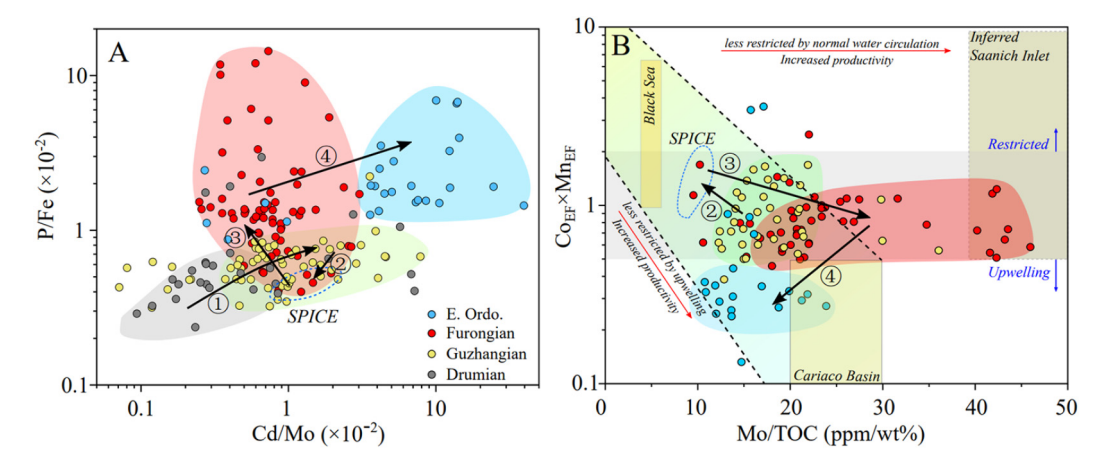


Fig. 5. A: Changes in the Cd/Mo ratio versus P/Fe ratio are used to reconstruct the intensity of primary productivity within the Baltoscandian Basin. ①: Drumian to Guzhangian; ② Guzhangian to Paibian (SPICE event); ③ Paibian to mid-late Furongian; and ④ mid-late Furongian to Tremadocian. B: Evolution of paleo-water circulation related to changes in paleo-productivity within the Baltoscandian Basin. The Mo/TOC ratio is used as an indicator of productivity and reducing conditions (Algeo and Lyons, 2006). The Mo/TOC ratio is 45 ± 5 in the Saanich Inlet, 25 ± 5 in the Cariaco Basin, and 4.5 ± 1 in the Black Sea. The $C_{EF}\times Mn_{EF}$ product is used as a proxy for water circulation (Sweere et al., 2016). The $C_{EF}\times Mn_{EF}$ product is mainly above 1 in the Black Sea, and below 0.5 in the Cariaco Basin. The area of Saanich Inlet was inferred due to the absence of reported Co and Mn values. In Fig. 5B, only samples with Mo concentrations exceeding 100 ppm were used to characterize euxinic conditions. The two yellow rectangles represent two modern euxinic basins: the Black Sea and Cariaco Basin. The dark yellow rectangle represents the features for the Sannich Inlet. Changes in water circulation and primary productivity are consistent with the three modern basins supporting our assumption (Black Sea: 63-135; Sannich Inlet: 490; Cariaco Basin: > 500 g C m⁻² year⁻¹; Sweere et al., 2016).

cumulation in the Alum Shale (Fig. 4A). During the Guzhangian Stage, redox conditions became sulfidic and remained euxinic conditions (Figs. 2C, 3E, and 4A), and the effects of Fe/Mn shuttle on Mo enrichment became weaker (Fig. 4A). During the Furongian, the Mo/Al ratio is above 10 ppm/%, indicating strongly sulfidic conditions (Figs. 2C and 3E). However, in the Early Ordovician, the reducing conditions weakened as the sulfide content decreased (Figs. 3E and 4A). These results indicate that redox conditions changed towards more sulfidic conditions from the Miaolingian to Furongian, followed by a sulfide-decreasing trend in the Early Ordovician (Fig. 4A). This is consistent with previously reported Mo isotopic variations that showed the δ^{98} Mo values increased from $\sim 0.4\%$ (median value) during the Drumian to $\sim 0.8\%$ during the Guzhangian Stage, and then increased to $\sim 1.0\%$ during the early Furongian (Fig. 4B; Gill et al., 2021).

5.1.2. Primary productivity

Phosphorus (P) is an essential nutrient for all forms of life on Earth, as it plays a fundamental role in many metabolic processes and is considered to have controlled marine primary productivity during Earth's history (Planavsky et al., 2010; Reinhard et al., 2016). The cycle of P is strongly affected by the burials of Fe and organic matter (Tribovillard et al., 2006; Scholz, 2018). Therefore, the P/Fe ratio is used to reconstruct productivity (Planavsky et al., 2010). In addition, the Cd/Mo ratio can differentiate the relative importance of the production of organic matter in the water column versus its preservation within sedimentary records (Sweere et al., 2016), because Cd is significantly correlated to primary productivity, whereas Mo is negligibly affected by biological activity (Chappaz et al., 2017). Here, we combined the Cd/Mo and P/Fe ratios to characterize paleo productivity (Fig. 5A). The results show that the 100P/Fe and Cd/Mo ratios increased from the Drumian to Guzhangian (Figs. 2F, 2G, and 5A), suggesting a higher productivity during the Guzhangian. Both proxies decreased slightly during the Steptoean Positive Carbon Isotope Excursion (SPICE) event in the Paibian Stage, followed by a significant increase in 100P/Fe but a rather small decrease in Cd/Mo during the mid-late Furongian (Fig. 5A). A non-trivial increase of nutrient inputs may have occurred, assuming the decrease of the Cd/Mo ratio is attributed to elevated Mo inputs from ocean water (Lehmann et al., 2007). The 100P/Fe and Cd/Mo ratios increased from the mid-late Furongian to Early Ordovician (Figs. 3C, 3D, and 5A), indicating a higher level of productivity that supported biological activity.

5.1.3. Water circulation

Plotting Mo concentration versus TOC is used to investigate the paleohydrographic conditions, particularly for anoxic depositional basins with restricted water circulation and limited water exchange (Algeo and Lyons, 2006; Hlohowskyj et al., 2021). Also, the product of Co enrichment factor by Mn enrichment factor (Co_{EF}×Mn_{EF}) can provide insights about water circulation in marine sedimentary environments because of a depletion in Co and Mn ions in upwelling systems from deep ocean water. Values below \sim 0.5 for the Co_{EF} \times Mn_{EF} represent an ocean water upwelling event (Sweere et al., 2016). Herein, we combined these two proxies and produced a new plot to assess water circulation in ancient anoxic basins with restricted water circulation (Figs. 5B and S8). This new approach provides not only information about water circulation but also additional evidence for identifying simultaneous changes in productivity. Our new results suggest that the water circulation became more restricted from the Guzhangian to the SPICE event in the Paibian Stage, and then became less restricted in the mid-late Furongian (Fig. 5B). During the Early Ordovician, the Mo/TOC ratios range from 10 to 25 ppm/wt%, while the Co_{EF}×Mn_{EF} values decrease below 0.5 (Fig. 5B), indicating an ocean water upwelling event. By comparing with modern marine basins (Fig. 5B; Black Sea, Cariaco Basin, and Saanich Inlet), we argue the productivity decreased from the Miaolingian to early Furongian and then gradually increased in the mid-late Furongian, which was followed by a relatively rapid increase in productivity during the Early Ordovician. This inference is also in accordance with the observed variations in organic productivity (Fig. 5A).

5.2. Global isotope chemostratigraphy

Global carbon and sulfur cycling are intimately coupled and can be directly linked to the long-term evolution of atmospheric and oceanic oxygenation throughout Earth's history (Gill et al., 2007; Fike et al., 2015; Guibourdenche et al., 2022). The relatively synchronous excursions of carbon and sulfur isotopic signatures measured in sedimentary records for numerous locations at the Earth' surface were successfully used to identify major environ-

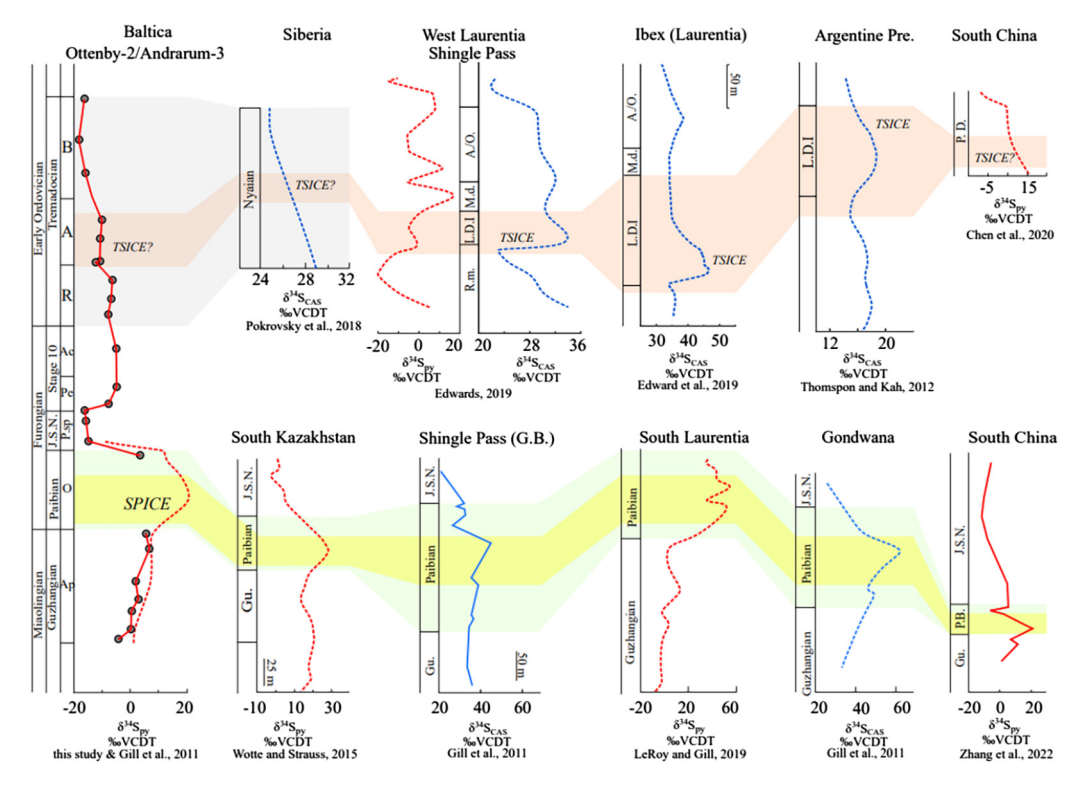


Fig. 6. Comparison of global sulfur isotopic signature during the SPICE and TSICE events. The light green zone, the yellow zone and the light red zone represent the Paibian Stage, the SPICE event, and the TSICE event, respectively. A continuous pyrite sulfur isotope ratios measurement across the Cambrian – Ordovician boundary is presented as dots in the left panel. The red curve is pyrite sulfur isotopes $(\delta^{34}S_{py})$, while the blue curve is sulfate sulfur isotopes $(\delta^{34}S_{CAS})$. The dashed curve is the median value calculated using a Lowess smoothing $(\alpha=0.15)$ by the PAST software package, and the non-dashed line is non-modeled due to the limitation of dataset. The detailed dataset and measured samples in other continents are provided in the Supplemental Material (Gill et al., 2011; Thompson and Kah, 2012; Pokrovsky et al., 2018; Edwards, 2019; Edwards et al., 2019; LeRoy and Gill, 2019; Wotte and Strauss, 2015; Chen et al., 2020; Zhang et al., 2022).

mental and biological changes (Gill et al., 2011; Saltzman et al., 2011; Cramer and Jarvis, 2020). Previous studies reported carbon isotopic signatures across the late Cambrian for Baltica and other paleo-continents, suggesting that there were synchronous carbon isotope excursions occurring at a global scale (Saltzman et al., 2011; Woods et al., 2011; Zhao et al., 2022). Herein, we compared organic carbon isotopes from the Ottenby-2 and DBH 15/73 cores to other Alum Shale cores. The regional correlation of organic carbon isotopes is presented in the Supplementary Information (Fig. S2).

In this study, we measured sulfur isotopes in two significant carbon isotope excursion events in the Furongian (SPICE event) and Early Ordovician (TSICE event: Top Skullrockian Isotope Carbon Excursion; Cramer and Jarvis, 2020). Owing to the limited sulfur isotope dataset reported and a lack of consensus (Landing et al., 2022), the sulfur isotopes data for the late Cambrian Hellnmaria-Red Tops Boundary/the Top Of Cambrian Excursion (HERB and TOCE) carbon excursion events are not included in this study. Sulfur isotopes during the SPICE event were previously reported for Baltica (Gill et al., 2011), Kazakhstan (Wotte and Strauss, 2015). Gondwana (South China and Australia: Saltzman et al., 2000: Zhang et al., 2022), and Laurentia (Gill et al., 2011; LeRoy and Gill, 2019). These prior results suggest that all paleo-continents display a roughly contemporaneous sulfur isotope excursion during the SPICE event. The comparison of sulfur isotopes for numerous paleo-continents is presented in Fig. 6. We, here, emphasize the comparison of sulfur isotopes during the TSICE event. We compiled the $\delta^{34}S_{CAS}$ and/or $\delta^{34}S_{py}$ from Baltica (Gill et al., 2011), Shingle Pass and Ibex of Laurentia (Edwards, 2019; Edwards et al., 2019), Argentine Precordillera (Thompson and Kah. 2012), Siberia (Pokrovsky et al., 2015), and South China (Chen et al., 2020). The correlation is based on the identified biostratigraphy and carbon

isotope chemostratigraphy (Supplementary Information and Figs. S3-S7; Cramer and Jarvis, 2020).

From the overall trend, the $\delta^{34}S_{py}$ values decreased progressively during the Tremadocian Alum Shale. This variation is similar to the modeled sulfur isotopic variation in Siberia (Pokrovsky et al., 2018). We consider that the negative sulfur isotopic variation is likely attributed to two mechanisms: (1) a decrease in sulfate reduction rate or (2) an increase in sulfate supply. Given that organic carbon isotope values, TOC, and total sulfur remain relatively stable in the Ottenby-2 core (Bian et al., 2022b), we excluded the first mechanism, assuming the availability of organic substrates for microbial sulfate reduction barely changed (e.g., Cao et al., 2016). In the Early Ordovician, the sedimentation rate decreased in Baltica (Fig. S1), indicating that continental sulfate input was not responsible for the increase in sulfate supply. Therefore, we argue that the sea-level rise mainly led to the negative sulfur isotopic change (Figs. 6 and 7E).

A weakly positive sulfur isotope excursion in Baltica is present during the TSICE event (Cramer and Jarvis, 2020). This excursion is also identified by the $\delta^{34} S_{py}$ of the Shingle Pass of Laurentia (Edwards, 2019) and the negative $\delta^{34} S_{py}$ excursion with a decreased derivative in South China (Chen et al., 2020). Moreover, the $\delta^{34} S_{CAS}$ in the Shingle Pass and Ibex of Laurentia shows a positive sulfur isotope excursion during the TSICE event (Thompson and Kah, 2012; Edwards, 2019; Edwards et al., 2019), which is consistent with the $\delta^{34} S_{CAS}$ excursion in Argentine Precordillera (Thompson and Kah, 2012). In addition, our measured sulfur isotope ratios show a continuously negative excursion prior to the TSICE event in Baltica. This variation is also recognized by the $\delta^{34} S_{py}$ and/or $\delta^{34} S_{CAS}$ in the Shingle Pass and Ibex of Laurentia (Edwards, 2019; Edwards et al., 2019) and Argentine Precordillera (Thompson and Kah, 2012).

Furthermore, Todd et al. (2019) investigated the paleo-environment of Bell Island Group in Avalonia, corresponding to the late Cambrian to early Florian Stages. They suggested that there was an upwelling of ocean water along the Avalonian continental shelf, probably stimulated by Ekman transport. Their conclusion is consistent with the water circulation in Baltica showing that the upwelling of ocean water supplied sulfate ions into reducing zones and led to a negative $\delta^{34}\mathrm{S}_{\mathrm{py}}$ excursion. Also, Vaucher et al. (2020) reported that oceanic plate subduction in the Cordillera Oriental closer to western Gondwana appeared to stimulate water exchange during the early Tremadocian, which could result in a negative $\delta^{34}\mathrm{S}_{\mathrm{py}}$ excursion. Hence, those evidence likely support the synchronous sulfur isotope excursion in a global context.

5.3. Spatial environmental dynamics in the Baltoscandian Basin

During the Miaolingian, the development of submarine sills contributed to the formation of the Baltoscandian Basin and the Alum Shale started to deposit (Nielsen and Schovsbo, 2015). From the Drumian to Guzhangian, the geochemical proxies for primary productivity display a consistent increase (Fig. 5A) that coincides with the rise in genus-level diversity (Harper et al., 2020). The increase in the $Co_{EF} \times Mn_{EF}$ values suggests the (seasonal) ocean water upwelling gradually disappeared and the water circulation became relatively restricted in the late Guzhangian (Fig. 2E). We infer that high primary productivity fueling oxygen demand and restricted water circulation decreasing exchange rate of oxygenated water led to anoxia in the water column (Meyer and Kump, 2008). This inference is also supported by the Mo and U geochemistry showing an evolution of redox conditions towards euxinia (Fig. 4B).

From the Miaolingian to early Furongian (Paibian Stage), sulfidic conditions became more intensive (Fig. 4A), the water circulation became more restricted (Fig. 5B), and simultaneously, the geochemical proxies for primary productivity decreased (Fig. 5A). Such a decrease in productivity could be attributed to two scenarios: (1) intensive sulfidic conditions that significantly enhanced Fe and Mo sequestrations (and thus do not necessarily represent a decreased productivity) or (2) a decreased biological productivity. Although we observe an increase in the Mo concentration, the decrease in the Cd concentration indicates a weaker biological productivity (Fig. 3E; Supplemental Table S2). Besides, the sulfidic conditions were not associated with an increase in Fe content (Supplemental Table S2). Therefore, the first scenario is excluded. A decrease in biological activity seems more reasonable because prior studies reported a decrease in genus-level diversity (Harper et al., 2020) and extinctions amongst trilobites and brachiopods during the SPICE event (Dahl et al., 2014). We hypothesize that high organic matter mineralization required a high oxygen supply that was limited at the time of deposition. These conditions speeded up the expansion of oxygen-deficient area in the water column and in turn, deteriorated the aquatic living conditions for the ecosystem. Additionally, the decreased terrestrial nutrient input, inferred from the declined sedimentation rate (Fig. S1), led to the decrease in the bioavailability of phosphorus and in productivity (Meyer and Kump, 2008). These conditions ultimately contributed to the biological extinction.

Despite high organic matter burial and the prevalence of extremely high sulfidic conditions in the mid-late Furongian (Figs. 2B and 4A; Bian et al., 2021), the high sedimentation rate indicates an increase in terrestrial nutrient inputs (Fig. S1). Besides, the water circulation were more vigorous (Fig. 5B). These conditions could result in enhanced biological productivity (Figs. 5A and 5B). By comparing with modern marine basins, the redox conditions were similar to the Black Sea in the early Furongian and to the Saanich Inlet in the mid-late Furongian, yet the two depositional environments displayed different primary productivity (Fig. 5B). The

increased productivity was contemporaneous with the significant phytoplankton diversification in the latest Cambrian (Servais et al., 2016).

From the Furongian to Early Ordovician, the declined sedimentation rate in the Alum Shale suggests a decreased input in terrestrial nutrients (Fig. S1). However, the synchronous water circulation changed to an upwelling current that could have brought deep-ocean nutrients to the ecosystem (Fig. 5B). In addition, the sea level rise and vigorous water exchange led to the mitigation of extremely sulfidic condition (Figs. 5B and 7E), which improved the living condition of the ecosystem. This change in water setting is analogous to the modern environmental shift from the Saanich Inlet to Cariaco Basin with enhanced primary productivity (Fig. 5B), which is coincident with the increased genus-level diversity and Early Ordovician zooplankton diversification (Harper and Servais, 2018).

5.4. Implications on global environmental and biological turnover

The Alum Shale has been widely investigated for understanding the late Cambrian – Early Ordovician environmental and biological covariation, probably because redox-sensitive metals in a macroscopic marine realm were sequestrated and precipitated in the Baltoscandian Basin (Gill et al., 2011; Zhao et al., 2022). Numerous studies have reported that the paleoenvironmental variations in the Baltoscandian Basin are similar to some affecting other continents (Sturesson et al., 2005; Gill et al., 2011, 2021; Dahl et al., 2014; Nielsen and Schovsbo, 2015; LeRoy et al., 2021; Bian et al., 2022a; Rooney et al., 2022; Zhao et al., 2022), laying the foundation of our assumption: the depositional variations of the Alum Shale reflect global (environmental and biological) changes.

In the Miaolingian, the intensive plate activity contributed to the formation of half-silled basins in the passive continental margins at a global scale, and simultaneously, the induced nutrientrich deep ocean water (upwelling) contributed to biological development (Figs. 2E and 7H). However, a negative consequence of increased productivity was to drive oxygen consumption exceeding its advective supplement in the water column (Murphy et al., 2000), leading to the formation of oxygen-deficient conditions (Figs. 4A, 4B, and 7G). Conditions favorable to sustain life were gradually deteriorating because of enhanced oxygen consumption by biological activity (Figs. 7A and 7B; Reinhard et al., 2016; Schobben et al., 2020), stagnated water circulation that diminished exchange rate of oxygenated water (Fig. 7E; Nishioka et al., 2020; Pohl et al., 2021), and high surface temperature that decreased oxygen dissolution in the water column (Fig. 7F; Zhang et al., 2018; Slater et al., 2019). These conditions were responsible for the early Furongian extinction event (Gill et al., 2011; Dahl et al.,

During early Jiangshanian, the sedimentary volcano-derived Hg anomaly, followed by recurrent extinction events, could be mainly associated with this bio-calamity (Figs. 7B, 7C and 7D; Dahl et al., 2014; Bian et al., 2022a). However, there were a declined proportion of extinction genera (Fig. 7B) and an increased metazoan generic diversity (Fig. 7A) during the mid-late Jiangshanian, indicating that the negative volcano-derived biological feedback was not maintained for a long time. The enhanced silicate weathering supported by elevated sedimentation rate (Fig. S1) was instead likely responsible for the increased biological productivity (Fig. 7H), as this phenomenon transferred additional terrestrial nutrients into the ecosystem and contributed to the decreased sea surface temperature (Figs. 7C and 7F; Penman et al., 2020; Goldberg et al., 2021). A consequence of the Earth's cooling was to provide conditions for the biota to move in shallow water areas, expanding the area of suitable habitat (Fig. 7G). Moreover, the intensified water circulation mitigated sulfidic conditions by the

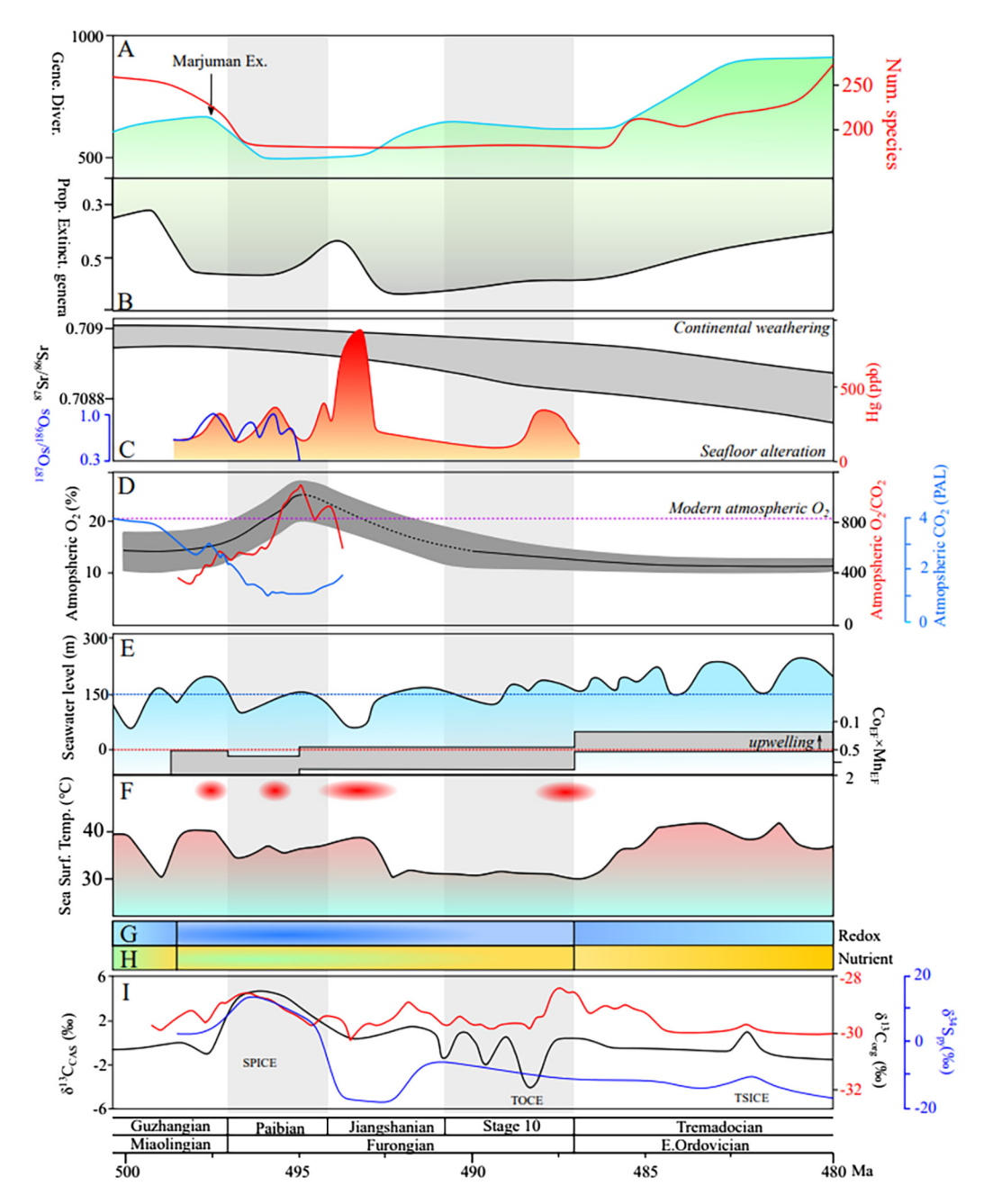


Fig. 7. A reconstruction of the biogeochemical changes from the Miaolingian to Early Ordovician. In Panel A, Gene. Diver.: global metazoan generic diversity; Marjuman Ex.: Marjuman extinction; and Num. species: Number of species. The light green line represents the cumulative generic diversity (left axis; Rasmussen et al., 2019; Zhao et al., 2022). Number of species (right axis; red line) is based on Fan et al. (2020). In Panel B, Prop. Extinct. Genera: proportion of extinction genera. The black line shows the proportion of extinction genera (left axis; Saltzman et al., 2015). In Panel C: The grey area is strontium isotope data (⁸⁷Sr/⁸⁵Sr) based on the LOWESS fitted line (left axis; McArthur et al., 2020). The blue curve shows osmium isotope data (¹⁸⁷Os/¹⁸⁶Os; left blue axis; Rooney et al., 2022). The red curve shows mercury (Hg) concentration (right axis; Bian et al., 2022a). In Panel D, The grey area shows the estimated atmospheric oxygen (left axis) from ~500 to ~495 Ma (Saltzman et al., 2011) and from ~490 to ~480 Ma (Edwards et al., 2017). The dashed black line is inferred by connecting the two periods. The atmospheric O₂/CO₂ ratio (right axis, red curve) and atmospheric CO₂ (right axis, blue curve) is based on Saltzman et al. (2011). In Panel E: the black curve shows meters above present-day seawater level (left axis; Rasmussen et al., 2019). The grey area shows the changes in water circulation change in Baltica (right axis). The dotted red line shows the threshold for upwelling of ocean water (Sweere et al., 2016). In Panel F: Surface Temp: oxygen-isotope-derived surface temperature. The curve used the estimated values with the lowest diagenetic alteration (Goldberg et al., 2021). The four red oval areas correspond to the recognized four Hg peaks in Panel C. Panel G shows the changes of redox condition in Baltica. The color changing from white to blue shows that the redox condition became more sulfidic. In Panel H, The color changing from light green to yellow shows the increased nutrient i

acceleration of water exchange (Fig. 7G), ultimately contributing to the increase in the marine metazoan generic diversity and the decrease in the proportion of extinction genera (Figs. 7A and 7B).

During the Early Ordovician (Tremadocian), although the sea surface temperature increased (Goldberg et al., 2021), the number of species continued to rise and the ratio of extinction genera showed a decrease (Figs. 7A and 7B; Saltzman et al., 2015; Fan et al., 2020). Our new data for Baltica suggest that despite a lower input of terrestrial nutrients, the elevated sea level accompanied by episodic upwelling events mitigated sulfidic conditions and at the same time, brought nutrients to the biota, speeding up the biological recovery.

6. Conclusions

We investigated various geochemical proxies in the Alum Shale for reconstructing the multi-variate paleo-environmental variations in the Baltoscandian Basin. Constrained by global carbon and sulfur isotopes, we extrapolated our findings to a global context and constructed the most comprehensive and high-resolution chemostratigraphy of the sedimentary records spanning through the late Cambrian - Early Ordovician. Our results show that depositional environments switched to sulfidic conditions, received low nutrient inputs and that the water circulation became more restricted from the Miaolingian to early Furongian. That succession of triggers was responsible for the globally recognized Steptoean Positive Carbon Isotope Excursion event. Later, intense volcanic activity resulted in recurrent biological calamity. This was followed by enhanced terrestrial weathering that provided higher inputs of terrestrial nutrients and contributed to the Earth's cooling across the mid-late Furongian, leading to an increased metazoan generic diversity. At the beginning of the Early Ordovician, despite reduced terrestrial nutrient input, massive oceanic water upwelling mitigated sulfidic conditions and brought nutrients to promote biological recovery. These environmental covariations were consistent with contemporaneous variations in the biosphere from the Miaolingian to Early Ordovician. We thus suggest that the covariation of surface temperature, nutrient inputs, and expansion/shrinkage of sulfidic bottom water, modulated by global tectonic activity, could have been responsible for the late Cambrian - Early Ordovician biological turnover.

CRediT authorship contribution statement

Leibo Bian: Conceptualization, sampling, methodology, data curation, and writing; **Anthony Chappaz:** Supervision, conceptualization, and writing; **Niels H. Schovsbo:** Supervision, sampling, data curation, and writing; **Xiaowei Wang:** Supervision, conceptualization, writing, and funding acquisition; **Wenzhi Zhao:** Supervision, conceptualization, methodology, and writing; and **Hamed Sanei:** Supervision, conceptualization, methodology, writing, and funding acquisition.

Declaration of competing interest

The authors declare that they have no known competing financial interests or personal relationships that could have appeared to influence the work reported in this paper.

Data availability

Data will be made available on request.

Acknowledgements

We acknowledge Editor Boswell Wing for handling this manuscript and Reviewers (Alexandre Pohl and one anonymous reviewer) for their insightful comments that greatly improved this paper. We also acknowledge Benjamin Gill for reviewing an earlier version of this study. This work was supported by the National Natural Science Foundation of China (42225303) and the National Key Research and Development Program of China (2022YFF0800304). The work was also funded by the '2021 William Spackman Student Research Award' of The Society for Organic Petrology (TSOP) granted to L.B., GeoCenter Denmark Project 2017-3 granted to N.S., ESF-EAR Grant 2051199 awarded to A.C., and State Key Laboratory of Organic Geochemistry (Grant No. SKLOG 202115) awarded to L.B., H.S., N.S., and A.C..

Appendix A. Supplementary material

Supplementary material related to this article can be found online at https://doi.org/10.1016/j.epsl.2023.118170.

References

- Algeo, T.J., Lyons, T.W., 2006. Mo-total organic carbon covariation in modern anoxic marine environments: implications for analysis of paleoredox and paleohydrographic conditions. Paleoceanography 21. https://doi.org/10.1029/2004pa001112.
- Algeo, T.J., Tribovillard, N., 2006. Environmental analysis of paleoceanographic systems based on molybdenum-uranium covariation. Chem. Geol. 268, 211–225.
- Algeo, T.J., Li, C., 2020. Redox classification and calibration of redox thresholds in sedimentary systems. Geochim. Cosmochim. Acta 287, 8–26.
- Babos, H.B., Stuart, S., Pluskowski, A., Brown, A., Rohrssen, M.K., Chappaz, A., 2019. Evidence for the onset of mining activities during the 13th century in Poland using lead isotopes from lake sediment cores. Sci. Total Environ. 683, 589–599.
- Bennett, W.W., Canfield, D.E., 2020. Redox-sensitive trace metals as paleoredox proxies: a review and analysis of data from modern sediments. Earth-Sci. Rev. 204, 103175.
- Bian, L., Schovsbo, N.H., Chappaz, A., Zheng, X., Nielsen, A.T., Ulrich, T., Wang, X., Dai, S., Galloway, J.M., Małachowska, A., Xu, X., Sanei, H., 2021. Molybdenumuranium-vanadium geochemistry in the lower Paleozoic Alum Shale of Scandinavia: implications for vanadium exploration. Int. J. Coal Geol. 239, 103730.
- Bian, L., Chappaz, A., Schovsbo, N.H., Nielsen, A.T., Sanei, H., 2022a. High Mercury enrichments in sediments from the Baltic continent across the late Cambrian: controls and implications. Chem. Geol. 599, 120846.
- Bian, L., Chappaz, A., Schovsbo, N.H., Sanei, H., 2022b. A new vanadium species in black shales: updated burial pathways and implications. Geochim. Cosmochim. Acta 338, 1–10.
- Breitburg, D., Levin, L.A., Oschlies, A., Grégoire, M., Chavez, F.P., Conley, D.J., Garçon, V., Gilbert, D., Gutiérrez, D., Isensee, K., Jacinto, G.S., 2018. Declining oxygen in the global ocean and coastal waters. Science 359, eaam7240.
- Cao, H., Kaufman, A.J., Shan, X., Cui, H., Zhang, G., 2016. Sulfur isotope constraints on marine transgression in the lacustrine Upper Cretaceous Songliao Basin, northeastern China. Palaeogeogr. Palaeoclimatol. Palaeoecol. 451, 152–163.
- Chappaz, A., Glass, J.B., Lyons, T.W., 2017. Molybdenum. In: White, W.M., Casey, W.H., Marty, B., Yurimoto, H. (Eds.), Encyclopedia of Geochemistry, vol. 2. Springer International, Cham, Switzerland, pp. 947–950.
- Chen, J., Montañez, I.P., Zhang, S., Isson, T.T., Macarewich, S.I., Planavsky, N.J., Zhang, F., Rauzi, S., Daviau, K., Yao, L., Qi, Y.P., 2022. Marine anoxia linked to abrupt global warming during Earth's penultimate icehouse. Proc. Natl. Acad. Sci. USA 119, e2115231119.
- Chen, K., Hu, D., Zhang, X., Zhu, H., Sun, L., Li, M., Shen, Y., 2020. Minor Δ^{33} S anomalies coincide with biotic turnover events during the Great Ordovician Biodiversification Event (GOBE) in South China. Glob. Planet. Change 184, 103069.
- Cramer, B., Jarvis, I., 2020. Carbon isotope stratigraphy. In: Geologic Time Scale 2020. Elsevier, pp. 309–343.
- Dahl, T.W., Boyle, R.A., Canfield, D.E., Connelly, J.N., Gill, B.C., Lenton, T.M., Bizzarro, M., 2014. Uranium isotopes distinguish two geochemically distinct stages during the later Cambrian SPICE event. Earth Planet. Sci. Lett. 401, 313–326.
- Edwards, C.T., 2019. Links between early Paleozoic oxygenation and the Great Ordovician Biodiversification Event (GOBE): a review. Palaeoworld 28, 37–50.
- Edwards, C.T., Saltzman, M.R., Royer, D.L., Fike, D.A., 2017. Oxygenation as a driver of the Great Ordovician Biodiversification Event. Nat. Geosci. 10, 925–929.
- Edwards, C.T., Fike, D.A., Saltzman, M.R., 2019. Testing carbonate-associated sulfate (CAS) extraction methods for sulfur isotope stratigraphy: a case study of a Lower–Middle Ordovician carbonate succession, Shingle Pass, Nevada, USA. Chem. Geol. 529, 119297.
- Evans, S.D., Tu, C., Rizzo, A., Surprenant, R.L., Boan, P.C., McCandless, H., Marshall, N., Xiao, S., Droser, M.L., 2022. Environmental drivers of the first major animal extinction across the Ediacaran White Sea-Nama transition. Proc. Natl. Acad. Sci. USA 119, e2207475119.
- Fan, J.X., Shen, S.Z., Erwin, D.H., Sadler, P.M., MacLeod, N., Cheng, Q.M., Hou, X.D., Yang, J., Wang, X.D., Wang, Y., Zhang, H., 2020. A high-resolution summary of Cambrian to Early Triassic marine invertebrate biodiversity. Science 367, 272–277.
- Fike, D.A., Bradley, A.S., Rose, C.V., 2015. Rethinking the ancient sulfur cycle. Annu. Rev. Earth Planet. Sci. 43, 593–622.
- Gill, B.C., Lyons, T.W., Saltzman, M.R., 2007. Parallel, high-resolution carbon and sulfur isotope records of the evolving Paleozoic marine sulfur reservoir. Palaeogeogr. Palaeoclimatol. Palaeoecol. 256, 156–173.
- Gill, B.C., Lyons, T.W., Young, S.A., Kump, L.R., Knoll, A.H., Saltzman, M.R., 2011. Geochemical evidence for widespread euxinia in the later Cambrian ocean. Nature 469, 80–83.
- Gill, B.C., Dahl, T.W., Hammarlund, E.U., LeRoy, M.A., Gordon, G.W., Canfield, D.E., Anbar, A.D., Lyons, T.W., 2021. Redox dynamics of later Cambrian oceans. Palaeogeogr. Palaeoclimatol. Palaeoecol. 581, 110623.

- Goldberg, S.L., Present, T.M., Finnegan, S., Bergmann, K.D., 2021. A high-resolution record of early Paleozoic climate. Proc. Natl. Acad. Sci. USA 118, e2013083118.
- Guibourdenche, L., Cartigny, P., Pierre, F.D., Natalicchio, M., Aloisi, G., 2022. Cryptic sulfur cycling during the formation of giant gypsum deposits. Earth Planet. Sci. Lett. 593, 117676.
- Harper, D.A., Servais, T., 2018. Contextualizing the onset of the Great Ordovician Biodiversification Event. Lethaia 51, 149–150.
- Harper, D.A., Cascales-Miñana, B., Servais, T., 2020. Early Palaeozoic diversifications and extinctions in the marine biosphere: a continuum of change. Geol. Mag. 157, 5–21.
- Hlohowskyj, S.R., Chappaz, A., Dickson, A.J., 2021. Molybdenum as a Paleoredox Proxy: Past, Present and Future. Elements in Geochemical Tracers in Earth System Science. Cambridge University Press.
- Jiao, W.J., Li, Y.X., Yang, Z.Y., 2018. Paleomagnetism of a well-dated marine succession in South China: a possible Late Cambrian true polar wander (TPW). Phys. Earth Planet. Inter. 277, 38–54.
- Krause, A.J., Mills, B.J., Zhang, S., Planavsky, N.J., Lenton, T.M., Poulton, S.W., 2018. Stepwise oxygenation of the Paleozoic atmosphere. Nat. Commun. 9, 1–10.
- Kröger, B., 2018. Changes in the latitudinal diversity gradient during the Great Ordovician Biodiversification Event. Geology 46, 127–130.
- Laakso, T.A., Schrag, D.P., 2014. Regulation of atmospheric oxygen during the Proterozoic. Earth Planet. Sci. Lett. 388, 81–91.
- Lafargue, E., Marquis, F., Pillot, D., 1998. Rock-Eval 6 applications in hydrocarbon exploration, production, and soil contamination studies. Oil Gas Sci. Technol. 53, 421–437
- Landing, E., Ripperdan, R.L., Geyer, G., 2022. Discussion of 'Reply to "Uppermost Cambrian carbon chemostratigraphy: the HERB and undocumented TOCE events are not synonymous". Geol. Mag. 159, 173–176.
- Lehmann, B., Nägler, T.F., Holland, H.D., Wille, M., Mao, J., Pan, J., Ma, D., Dulski, P., 2007. Highly metalliferous carbonaceous shale and Early Cambrian seawater. Geology 35, 403–406.
- LeRoy, M.A., Gill, B.C., 2019. Evidence for the development of local anoxia during the Cambrian SPICE event in eastern North America. Geobiology 17, 381–400.
- LeRoy, M.A., Gill, B.C., Sperling, E.A., McKenzie, N.R., Park, T.-Y.S., 2021. Variable redox conditions as an evolutionary driver? A multi-basin comparison of redox in the middle and later Cambrian oceans (Drumian-Paibian). Palaeogeogr. Palaeoclimatol. Palaeoecol. 566, 110209.
- Lu, Z., Hoogakker, B.A., Hillenbrand, C.D., Zhou, X., Thomas, E., Gutchess, K.M., Lu, W., Jones, L., Rickaby, R.E., 2016. Oxygen depletion recorded in upper waters of the glacial Southern Ocean. Nat. Commun. 7, 1–9.
- Lyons, T.W., Diamond, C.W., Planavsky, N.J., Reinhard, C.T., Li, C., 2021. Oxygenation, life, and the planetary system during Earth's middle history: an overview. Astrobiology 21, 906–923.
- McArthur, J.M., Howarth, R.J., Shields, G.A., Zhou, Y., 2020. Strontium isotope stratigraphy. In: Geologic Time Scale 2020. Elsevier, pp. 211–238.
- Meyer, K.M., Kump, L.R., 2008. Oceanic euxinia in Earth history: causes and consequences. Annu. Rev. Earth Planet. Sci. 36, 251–288.
- Murphy, A.E., Sageman, B.B., Hollander, D.J., Lyons, T.W., Brett, C.E., 2000. Black shale deposition and faunal overturn in the Devonian Appalachian Basin: clastic starvation, seasonal water-column mixing, and efficient biolimiting nutrient recycling. Paleoceanography 15, 280–291.
- Nielsen, A.T., Schovsbo, N.H., 2015. The regressive Early-Mid Cambrian 'Hawke Bay Event' in Baltoscandia: epeirogenic uplift in concert with eustasy. Earth-Sci. Rev. 151, 288–350.
- Nishioka, J., Obata, H., Ogawa, H., Ono, K., Yamashita, Y., Lee, K., Takeda, S., Yasuda, I., 2020. Subpolar marginal seas fuel the North Pacific through the intermediate water at the termination of the global ocean circulation. Proc. Natl. Acad. Sci. USA 117, 12665–12673.
- Oschlies, A., Brandt, P., Stramma, L., Schmidtko, S., 2018. Drivers and mechanisms of ocean deoxygenation. Nat. Geosci. 11, 467–473.
- Penman, D.E., Rugenstein, J.K.C., Ibarra, D.E., Winnick, M.J., 2020. Silicate weathering as a feedback and forcing in Earth's climate and carbon cycle. Earth-Sci. Rev. 209, 103298.
- Planavsky, N.J., Rouxel, O.J., Bekker, A., Lalonde, S.V., Konhauser, K.O., Reinhard, C.T., Lyons, T.W., 2010. The evolution of the marine phosphate reservoir. Nature 467, 1088–1090.
- Pohl, A., Lu, Z., Lu, W., Stockey, R.G., Elrick, M., Li, M., Desrochers, A., Shen, Y., He, R., Finnegan, S., Ridgwell, A., 2021. Vertical decoupling in Late Ordovician anoxia due to reorganization of ocean circulation. Nat. Geosci. 14. 868–873.
- Pokrovsky, B.G., Zaitsev, A.V., Dronov, A.V., Bujakaite, M.I., Timokhin, A.V., Petrov, O.L., 2018. C, O, S, and Sr isotope geochemistry and chemostratigraphy of Ordovician sediments in the Moyero River Section, Northern Siberian Platform. Lithol. Miner. Resour. 53, 283–306.
- Rasmussen, C.M.Ø., Kröger, B., Nielsen, M.L., Colmenar, J., 2019. Cascading trend of Early Paleozoic marine radiations paused by Late Ordovician extinctions. Proc. Natl. Acad. Sci. USA 116, 7207–7213.
- Reinhard, C.T., Planavsky, N.J., Olson, S.L., Lyons, T.W., Erwin, D.H., 2016. Earth's oxygen cycle and the evolution of animal life. Proc. Natl. Acad. Sci. USA 113, 8933–8938.

- Reinhard, C.T., Planavsky, N.J., Gill, B.C., Ozaki, K., Robbins, L.J., Lyons, T.W., Fischer, W.W., Wang, C., Cole, D.B., Konhauser, K.O., 2017. Evolution of the global phosphorus cycle. Nature 541, 386–389.
- Rico, K.I., Sheldon, N.D., Gallagher, T.M., Chappaz, A., 2019. Molybdenum availability, productivity, and atmospheric oxygen in the Mesoproterozoic. Geophys. Res. Lett. 46, 5871–5878.
- Rooney, A.D., Millikin, A.E., Ahlberg, P., 2022. Re-Os geochronology for the Cambrian SPICE event: insights into euxinia and enhanced continental weathering from radiogenic isotopes. Geology 50, 716–720.
- Saltzman, M.R., Ripperdan, R.L., Brasier, M.D., Lohmann, K.C., Robison, R.A., Chang, W.T., Peng, S., Ergaliev, E.K., Runnegar, B., 2000. A global carbon isotope excursion (SPICE) during the Late Cambrian: relation to trilobite extinctions, organic-matter burial and sea level. Palaeogeogr. Palaeoclimatol. Palaeoecol. 162, 211–223.
- Saltzman, M.R., Young, S.A., Kump, L.R., Gill, B.C., Lyons, T.W., Runnegar, B., 2011.
 Pulse of atmospheric oxygen during the late Cambrian. Proc. Natl. Acad. Sci.
 USA 108, 3876–3881.
- Saltzman, M.R., Edwards, C.T., Adrain, J.M., Westrop, S.R., 2015. Persistent oceanic anoxia and elevated extinction rates separate the Cambrian and Ordovician radiations. Geology 43, 807–810.
- Sanei, H., Petersen, H., Schovsbo, N., Jiang, C., Goodsite, M.E., 2014. Petrographic and geochemical composition of kerogen in the Furongian (U. Cambrian) Alum Shale, central Sweden: reflections on the petroleum generation potential. Int. J. Coal Geol. 132, 158–169.
- Schobben, M., Foster, W.J., Sleveland, A., Zuchuat, V., Svensen, H.H., Planke, S., Bond, D.P., Marcelis, F., Newton, R.J., Wignall, P.B., Poulton, S.W., 2020. A nutrient control on marine anoxia during the end-Permian mass extinction. Nat. Geosci. 13, 640–646.
- Scholz, F., 2018. Identifying oxygen minimum zone-type biogeochemical cycling in Earth history using inorganic geochemical proxies. Earth-Sci. Rev. 184, 29–45.
- Schovsbo, N.H., Nielsen, A.T., Gautier, D.L., 2014. The lower Palaeozoic shale gas play in Denmark. GEUS Bull. 31, 19–22.
- Servais, T., Perrier, V., Danelian, T., Klug, C., Martin, R., Munnecke, A., Nowak, H., Nützel, A., Vandenbroucke, T.R., Williams, M., Rasmussen, C.M., 2016. The onset of the 'Ordovician Plankton Revolution' in the late Cambrian. Palaeogeogr. Palaeoclimatol. Palaeoecol. 458, 12–28.
- Scotese, C.R., 2014. Atlas of Cambrian and Early Ordovician paleogeographic maps (Mollweide Projection). In: The Early Paleozoic, PALEOMAP Atlas for ArcGIS, Maps 81–88, Vol. 5, PALEOMAP Project, Evanston, IL.
- Slater, S.M., Twitchett, R.J., Danise, S., Vajda, V., 2019. Substantial vegetation response to early Jurassic global warming with impacts on oceanic anoxia. Nat. Geosci. 12, 462–467.
- Sturesson, U., Popov, L.E., Holmer, L.E., Bassett, M.G., Felitsyn, S., Belyatsky, B., 2005. Neodymium isotopic composition of Cambrian–Ordovician biogenic apatite in the Baltoscandian Basin: implications for palaeogeographical evolution and patterns of biodiversity. Geol. Mag. 142, 419–439.
- Sweere, T., van den Boorn, S., Dickson, A.J., Reichart, G.J., 2016. Definition of new trace-metal proxies for the controls on organic matter enrichment in marine sediments based on Mn, Co, Mo and Cd concentrations. Chem. Geol. 441, 235–245.
- Taylor, S.R., McLennan, S.M., 1985. The continental crust: its composition and evolution.
- Thompson, C.K., Kah, L.C., 2012. Sulfur isotope evidence for widespread euxinia and a fluctuating oxycline in Early to Middle Ordovician greenhouse oceans. Palaeogeogr. Palaeoclimatol. Palaeoecol. 313, 189–214.
- Todd, S.E., Pufahl, P., Murphy, J., Taylor, K., 2019. Sedimentology and oceanography of Early Ordovician ironstone, Bell Island, Newfoundland: Ferruginous seawater and upwelling in the Rheic Ocean. Sediment. Geol. 379, 1–15.
- Tribovillard, N., Algeo, T.J., Lyons, T., Riboulleau, A., 2006. Trace metals as paleoredox and paleoproductivity proxies: an update. Chem. Geol. 232, 12–32.
- Tribovillard, N., Algeo, T.J., Baudin, F., Riboulleau, A., 2012. Analysis of marine environmental conditions based on molybdenum-uranium covariation—applications to Mesozoic paleoceanography. Chem. Geol. 324, 46–58.
- Trotter, J.A., Williams, I.S., Barnes, C.R., Lécuyer, C., Nicoll, R.S., 2008. Did cooling oceans trigger Ordovician biodiversification? Evidence from conodont thermometry. Science 321, 550–554.
- Trubovitz, S., Stigall, A.L., 2016. Synchronous diversification of Laurentian and Baltic rhynchonelliform brachiopods: implications for regional versus global triggers of the Great Ordovician Biodiversification Event. Geology 44, 743–746.
- Vaucher, R., Vaccari, N.E., Balseiro, D., Muñoz, D.F., Dillinger, A., Waisfeld, B.G., Buatois, L.A., 2020. Tectonic controls on late Cambrian-Early Ordovician deposition in cordillera oriental (northwest Argentina). Int. J. Earth Sci. 109, 1897–1920.
- Woods, M.A., Wilby, P.R., Leng, M.J., Rushton, A.W., Williams, M., 2011. The furongian (late Cambrian) steptoean positive carbon isotope excursion (SPICE) in Avalonia. J. Geol. Soc. 168, 851–862.
- Wotte, T., Strauss, H., 2015. Questioning a widespread euxinia for the Furongian (Late Cambrian) SPICE event: indications from δ^{13} C, δ^{18} O, δ^{34} S and biostratigraphic constraints. Geol. Mag. 152, 1085–1103.
- Zhang, F., Romaniello, S.J., Algeo, T.J., Lau, K.V., Clapham, M.E., Richoz, S., Herrmann, A.D., Smith, H., Horacek, M., Anbar, A.D., 2018. Multiple episodes of extensive

marine anoxia linked to global warming and continental weathering following the latest Permian mass extinction. Sci. Adv. 4, e1602921.

Zhang, L., Algeo, T.J., Zhao, L., Chen, Z.Q., Zhao, H., Zhang, Z., Li, C., 2022. Linkage of the late Cambrian microbe-metazoan transition (MMT) to shallow-marine oxygenation during the SPICE event. Glob. Planet. Change 213, 103798.

Zhao, Z., Thibault, N.R., Dahl, T.W., Schovsbo, N.H., Sørensen, A.L., Rasmussen, C.M., Nielsen, A.T., 2022. Synchronizing rock clocks in the late Cambrian. Nat. Commun. 13, 1–11.